Neuron
Article

A Parturition-Associated Nonsynaptic Coherent Activity Pattern in the Developing Hippocampus

Valérie Crépel,[1] Dmitriy Aronov,[2] Isabel Jorquera,[1] Alfonso Represa,[1] Yehezkel Ben-Ari,[1] and Rosa Cossart[1,*]
[1] INMED, INSERM, U29, Université de La Méditerranée, Parc scientifique de Luminy, BP 13, 13273 Marseille Cedex 09, France
[2] Massachusetts Institute of Technology, 77 Massachusetts Avenue, Cambridge, MA 02139 USA
*Correspondence: cossart@inmed.univ-mrs.fr
DOI 10.1016/j.neuron.2007.03.007

SUMMARY

Correlated neuronal activity is instrumental in the formation of networks, but its emergence during maturation is poorly understood. We have used multibeam two-photon calcium microscopy combined with targeted electrophysiological recordings in order to determine the development of population coherence from embryonic to postnatal stages in the hippocampus. At embryonic stages (E16–E19), synchronized activity is absent, and neurons are intrinsically active and generate L-type channel-mediated calcium spikes. At birth, small cell assemblies coupled by gap junctions spontaneously generate synchronous nonsynaptic calcium plateaus associated to recurrent burst discharges. The emergence of coherent calcium plateaus at birth is controlled by oxytocin, a maternal hormone initiating labour, and progressively shut down a few days later by the synapse-driven giant depolarizing potentials (GDPs) that synchronize the entire network. Therefore, in the developing hippocampus, delivery is an important signal that triggers the first coherent activity pattern, which is silenced by the emergence of synaptic transmission.

INTRODUCTION

During brain maturation, networks shift from an ensemble of cells endowed with sparse spontaneous activity to a collection of neuronal microcircuits communicating by means of thousands of synapses to generate complex spike patterns that are behaviorally relevant. During this process, emerging networks engage in a sequential maturation of coordinated activity that is believed to control the formation of region-specific synaptic connections (Colin-Le Brun et al., 2004; Garaschuk et al., 2000; Kasyanov et al., 2004) as well as the organization and shaping of sensory and motor systems (Cang et al., 2005; Kandler and Gillespie, 2005; Katz and Shatz, 1996; Khazipov et al., 2004). Initially restricted to pairs of neurons (Owens and Kriegstein, 1998), correlated activity gets more complex, involving larger ensembles of neurons as the network matures and the density of functional synapses augments. Spontaneous correlated neuronal activity clearly represents the hallmark of the developing brain since it has been observed in a wide range of peripheral (Galli and Maffei, 1988; Meister et al., 1991; O'Donovan, 1989; Syed et al., 2004) and central (Ben Ari, 2001, 2002; Ben Ari et al., 1989; Garaschuk et al., 2000; Kandler and Katz, 1998; Owens and Kriegstein, 1998; Palva et al., 2000; Yuste et al., 1992) structures.

In developing cortical structures, several patterns of coherent activity have been described at different stages, thus providing a general framework of network maturation. At embryonic stages, locally coordinated calcium events can be observed in migrating neurons (Owens and Kriegstein, 1998). Later, spatially constrained coordinated calcium activity synchronizes gap-junction-connected neighboring neurons, independently from synaptic transmission (Dupont et al., 2005; Kandler and Katz, 1998; Owens and Kriegstein, 1998; Yuste et al., 1992) or not (Corlew et al., 2004; Dupont et al., 2005). However, they are rare events, and their study therefore required the use of pharmacological manipulation to induce them (high potassium, low magnesium, temperature drop, activation of muscarinic receptors, etc.) (Dupont et al., 2005; Kandler and Katz, 1998; Yuste et al., 1992). Then, large groups of neighboring neurons engage in synchronous network events by means of synaptic transmission (Ben Ari, 2002; Ben Ari et al., 1989; Garaschuk et al., 2000; Khazipov et al., 2001; McCabe et al., 2006; Palva et al., 2000) as well as intrinsic voltage-gated currents (Corlew et al., 2004; Sipila et al., 2005). This universally observed widespread synchrony (Ben Ari, 2001) provides most of the activity during a restricted time window of postnatal development (Ben Ari et al., 1989; Corlew et al., 2004; Garaschuk et al., 2000) before being replaced by behaviorally relevant oscillatory patterns.

In spite of this considerable information, the maturation of population coherence in the brain is not fully understood. First, at the cellular level, the electrophysiological correlates of nonsynaptic coherent activity patterns have not been described. Second, it is not known whether

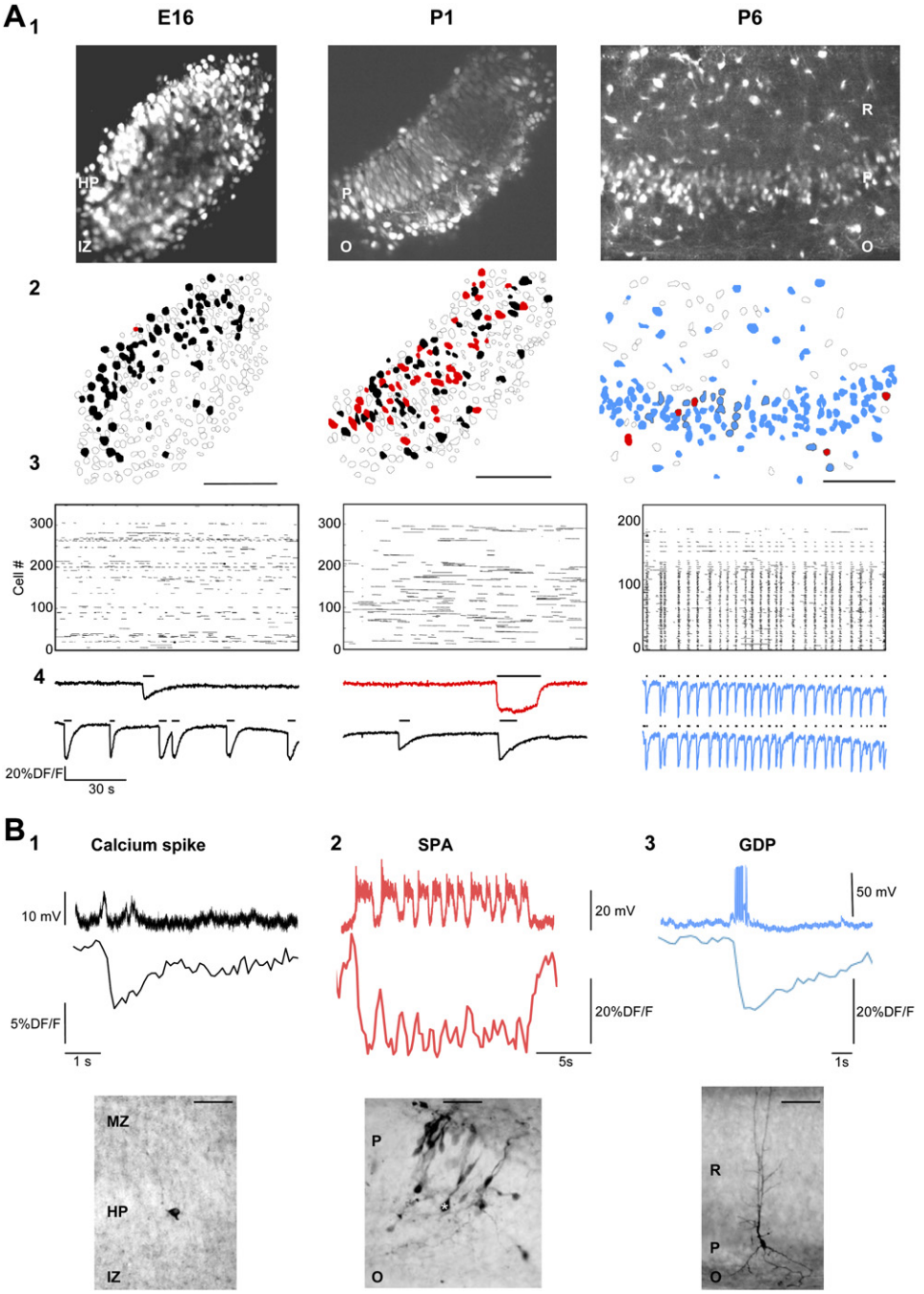

Figure 1. Multibeam Two-Photon Imaging of the Three Dominant Forms of Primary Activity in the CA1 Region from Embryonic Stages to First Postnatal Days

(A1) Two-photon calcium fluorescence images of the CA1 region from mouse hippocampal slices at E16, P1, and P6. Time resolution: 100 ms/frame. For corresponding movies, see Movies S1 and S2. (A2) Automatically detected contours of the cells from the fluorescence images. Open contours indicate silent cells. Black-filled contours indicate cells producing calcium spikes, red-filled contours are cells producing calcium plateaus (SPA cells), and blue-filled contours are cells producing fast synchronous calcium transients (GDP events). Scale bars, 100 μm. (A3) Rasterplots of the activity from the three movies illustrated in (A1) (control ACSF). Each row represents a single cell, and each horizontal line the duration of detected calcium transients (see Experimental Procedures). (A4) Three populations of events can be distinguished as shown by their representative fluorescence traces (black, calcium spikes; red, calcium plateaus, i.e., SPAs; blue, GDP events).

(B) Simultaneous current-clamp (Vrest ~−60 mV, top) and optical recordings (bottom trace) in three representative neurons for the three types of calcium activities described in (A). Bottom pictures are photomicrographs of the biocytin-filled neurons recorded above. Scale bars, 50 μm (left

distinct coherent events such as localized and widespread synchronous activities coexist and interact during circuit maturation. It is also essential to determine whether delivery and other pivotal biological developmental steps control the evolution of network patterns. The aims of the present study were therefore to investigate the development of population coherence both at the network and cellular levels within the same cortical network and to determine its correlation with delivery and postnatal maturation.

We have determined in detail the maturation of correlated activity in the developing hippocampus, a region where the maturation of GABA and glutamate receptors and synapse-driven patterns have been extensively described (Ben Ari, 2002). We used a quantitative approach that enabled us to record the activity of a large number of identified neurons in order to determine their contribution to correlated activities without an a priori assumption. Fast multibeam two-photon calcium microscopy (Nielsen et al., 2001) combined with targeted electrophysiological recordings was implemented here for the first time (to our knowledge). We recorded the activity of large networks with a cellular resolution that allows the detection of discrete coherent patterns and identified their cellular correlates (Cossart et al., 2003). We report that, at embryonic stages, neurons are intrinsically active and sporadically generate voltage-gated calcium spikes. Around birth, a remarkable coordinated activity pattern emerges: small groups of intrinsically active neurons couple by gap junctions and generate synchronous, nonsynaptic calcium plateaus. Such coherent calcium activity is produced by sustained periods of recurrent burst discharges (<1 Hz, for tens of seconds) dependent on the activation of L-type calcium and sodium channels and on the cationic current Ih. Since we observed the emergence of population coherence at birth, we hypothesized that it is related to parturition and in particular to oxytocin. This maternal hormone, released during delivery (Gimpl and Fahrenholz, 2001) and which easily reaches the fetus (Malek et al., 1996), was recently shown to induce a transient excitatory-to-inhibitory switch in GABA actions in the fetal brain shortly before delivery (Tyzio et al., 2006). Accordingly, we demonstrate that the first coherent activity pattern dominating the hippocampal network at birth is boosted up by oxytocin. Furthermore, we establish that similar mechanisms underlie the near-term enhancement of population coherence and the oxytocin-mediated switch in GABA signaling. The handover of network synchrony from local nonsynaptic to widespread synapse-driven activities (GDPs) occurs *progressively* during the first postnatal week, since both dynamics coexist during a critical period. Blocking GDPs reinstates the synchronous primitive nonsynaptic burst discharges, suggesting that both events are mutually exclusive. Thus, delivery triggers the first coherent activity in gap-junction-coupled cell assemblies in the form of calcium plateaus nesting nonsynaptic burst discharges. This primitive pattern is shut off by the emergence of synaptic transmission.

RESULTS

To acquire a dynamic and quantitative estimate of the activity of a large number of neurons, we used large-scale two-photon calcium microscopy in mouse hippocampal slices (Cossart et al., 2003, 2005). Since the major limitation of imaging techniques is time resolution, we have used a novel system based on multibeam scanning of the preparation, which achieves millisecond resolution and reliably detects single action potentials. We recorded movies of spontaneous activity in slices of mouse hippocampus aged between E16 and P14 and focused on the CA1 region (field size: 430 × 380 μm^2; 135–560 cells, average: 274 cells per movie; 76,107 neurons recorded in total). Analysis was performed online using custom software to measure fluorescence changes in each hippocampal cell and mark the onset and offset of individual calcium transients (Figure 1; see also Experimental Procedures). We then combined calcium transients from all cells into raster plots indicating the activity of each imaged cell as a function of time (Figure 1).

With this compound approach, we determined the number of neurons participating in a given network pattern and described their temporal and spatial links. Neurons involved in the generation of network activities were targeted for whole-cell recordings to determine the physiological properties underlying such events (Figure 1). Recorded neurons were filled with dyes for post hoc morphological identification (Figure 1).

Population Coherence Emerges at Birth in Developing Hippocampal Neurons

We first determined the patterns of activity most represented at three sequential developmental stages using calcium imaging and targeted current-clamp recordings from active neurons: embryo (E16–E19), around birth (P0–P2), and postnatal (P6–P10). Spontaneous calcium events were sorted both manually and automatically based on their kinetics, blindly to the experimental condition (see Experimental Procedures). We found three successive dominant types of calcium dynamics:

(1) At embryonic stages (E16–E19), only a minority of cells were active (21% ± 1%, n = 11 slices, 3832 cells). All activity consisted of sporadic brief calcium events (2.95 ± 0.04 s duration, n = 7000 events, Figures 1 and 2) that were poorly correlated between neurons (0.54% cell pairs significantly correlated, see Experimental Procedures). Current-clamp

and middle), 100 μm (right). (B1) Black, calcium spikes recorded in a neuron at E16. (B2) Red, SPA recorded in a neuron at P0. Note that biocytin-filling of a single cell (*) results in the labeling of groups of neurons. (B3) Blue, GDP; labeled cell is a typical CA1 pyramidal neuron. HP, hippocampal plate; IZ, intermediate zone; MZ, marginal zone; O, stratum oriens; P, stratum pyramidale; R, stratum radiatum.

recordings from active neurons revealed that these calcium events corresponded to immature membrane-potential spikes (Figure 1). We will refer to these early calcium events as calcium spikes.

(2) Around birth (P0–P2), more cells generated calcium spikes (see Movie S1 in the Supplemental Data available online), but another pattern appeared in about 20% of active cells consisting of long-lasting calcium plateaus (duration: 9.1 ± 0.1 s, 0.02 Hz, n = 5893 events, significantly different from calcium spikes in terms of duration, Kolmogorov-Smirnov, $p < 0.001$; Figures 1 and 2). These plateaus produced recurrent burst discharges when cells were recorded at Vrest, as shown by targeted whole-cell recordings (Vm = −61 ± 1 mV, ΔV = 12 ± 4 mV, 0.5 ± 0.2 Hz, n = 12 cells, Figures 1 and 4). In contrast to calcium spikes, the onsets of calcium plateaus were significantly synchronized between neurons within a 200 ms time window (7.8% pairs of calcium plateaus correlated versus 1.3% calcium spikes pairs, $p < 0.05$, Figures 6 and 8). On average, synchronous calcium plateaus involved 3.0 ± 0.2 neurons; per movie, the largest synchronous events comprised 7.4 ± 1.9 neurons (n = 11 slices, 384 cells producing plateaus). Synchronous events occurred on average 7 ± 1 times per min (n = 11 slices). The synchronous occurrence of calcium plateaus in a subpopulation of neurons represents the first coherent activity pattern in the hippocampus. We propose to refer to this primary coherent activity, characterized by the occurrence of synchronous calcium plateaus in neuronal assemblies as SPA (synchronous plateau assemblies).

(3) At later postnatal stages (P6–P10), a majority of cells (64% ± 4%) were active in a strongly coordinated manner (21.1% pairs significantly correlated, peaks of synchronous activation involving up to 80% of imaged cells, n = 30 slices, $p < 0.05$; Figure 1, see Movie S2). This activity corresponds to the well-described GDPs (Ben Ari et al., 1989), as revealed by current-clamp recordings (Figure 1) and by their blockade by $GABA_A$ and glutamate receptor antagonists (Figure 3).

We conclude that three patterns, differing both by their calcium dynamics and their electrophysiological correlates, dominate early spontaneous activity in the CA1 region: uncorrelated isolated spikes, synchronized calcium plateaus nesting recurrent burst discharges (SPAs), and a pattern corresponding to the synapse-driven GDPs. The developmental incidence of calcium spikes, SPAs, and GDPs also differed: uncorrelated spikes were the dominant pattern at embryonic stages (E16–E19) and was then progressively replaced by SPAs and GDPs that prevailed by the end of the first postnatal week (Figure 2). Both SPAs and GDPs disappear after the second postnatal week (Figure 2). Therefore, population coherence emerges at birth in the hippocampus in the transient

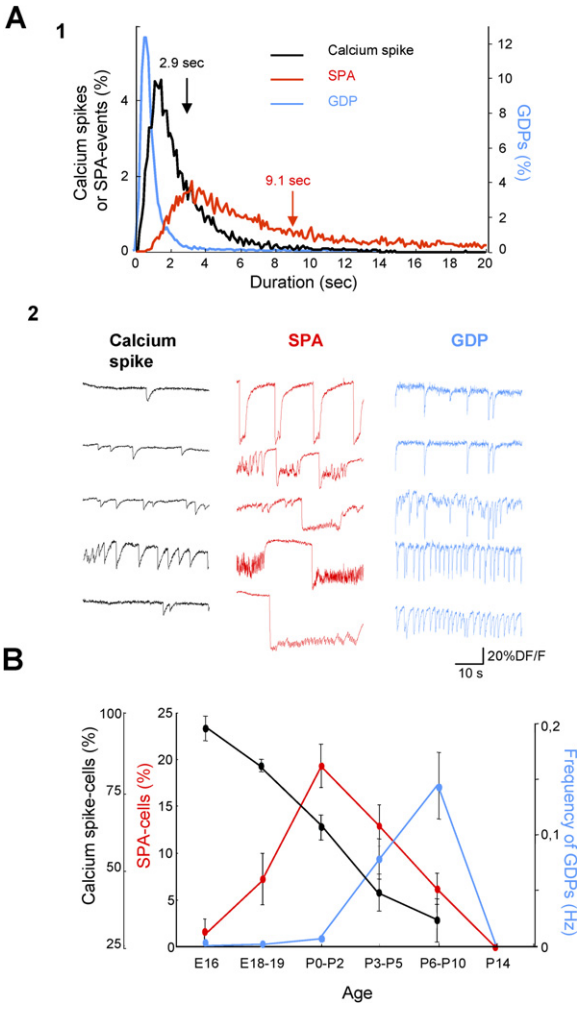

Figure 2. Dynamics and Developmental Features of the Three Dominant Forms of Primary Activity in the CA1 Region

(A1) Distribution plot of the durations of calcium transients for the three types of primary activities reveals three distinct populations (Kolmogorov-Smirnov, $p < 0.001$). (A2) Representative calcium fluorescence traces for calcium spikes, two and three measured in neurons from different movies. Note that first two and bottom three highly synchronized GDP traces are from the same movie.

(B) Graph indicates the fraction of calcium-spike cells (black), SPA cells (red) relative to the number of active cells, as well as the frequency of GDPs (blue), for six successive age groups. Error bars indicate SEMs.

form of SPAs involving bursting neuronal assemblies. We next investigated the cellular mechanisms responsible for the generation of the two dominating patterns from E16 until birth, calcium spikes and SPAs.

Intrinsic Voltage-Gated Ionic Conductances Generate Calcium Spikes and SPAs

Sporadic calcium spikes were intrinsically generated by high-threshold calcium conductances with a contribution of sodium channels since (1) L-type calcium (10 μM nifedipine) and sodium (1 μM TTX) channel antagonists

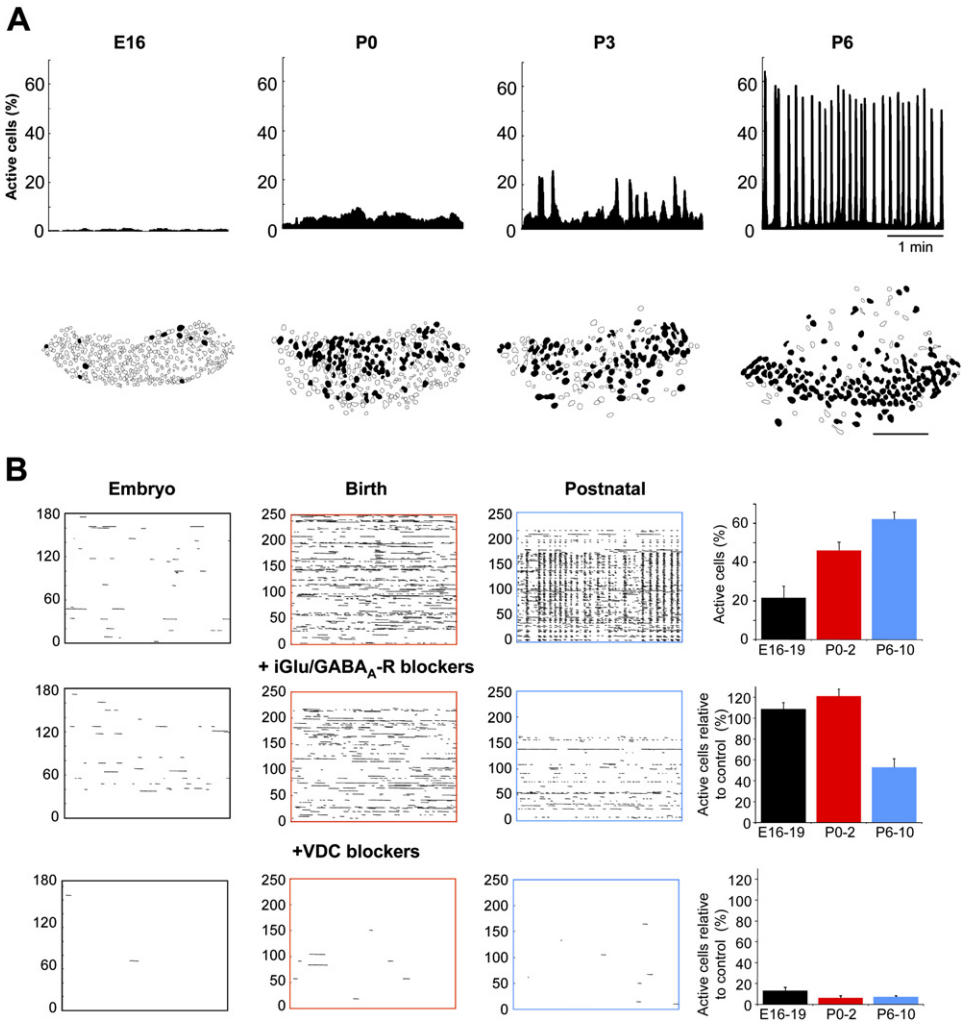

Figure 3. Pharmacological Properties of the Three Dominant Forms of Primary Activity in the CA1 Hippocampus

(A) Representative histograms showing the percentage of imaged cells that are detected as being active (active cells [%]) at each movie frame from E16 to P6 (time resolution: 100 ms). Peaks of activity in the network are GDPs. There is a clear increase in the amplitude (i.e., fraction of cells coactive at peaks of synchrony) and in the frequency of GDPs. Filled contours mark cells detected as being active at least once during the recording time corresponding to the above histograms. Note that whereas synchrony dramatically increases between P1 and P6, the fraction of active cells is comparable. In contrast, very few neurons are active at E16.

(B) Representative rasterplots of calcium event duration recorded at E16 (embryo, black), P0 (birth, red), and P6 (postnatal, blue) in control (top), in the presence of blockers for glutamatergic and GABAergic transmission (middle, see Experimental Procedures), and in the presence of voltage-dependent sodium and L-type calcium channel (VDC) blockers (bottom, 1 μM TTX and 10 μM nifedipine). Histograms show the averaged fraction of imaged cells detected as active at least once in a movie frame in the three different pharmacological conditions for the three age groups (E16–E19, black), (P0–P2, red), and (P6–P10, blue). Note that histograms in the presence of blockers are expressed relative to control activities. Error bars indicate SEMs.

strongly reduced these events (Figure 3). Before birth (E16–E19), the fraction of active cells displaying calcium spikes, "fraction of calcium-spike cells," was reduced by nifedipine (10 μM) alone to 22% ± 10% of control; further addition of TTX reduced the fraction of calcium-spike cells to 15% ± 4% of control (n = 7 slices, 2058 cells, Figure 3). At later stages (P3–P10), both nifedipine and TTX were required to reduce the fraction of calcium-spike cells to 11% ± 1% of control (n = 7 slices, 1476 cells, Figure 3). Interestingly, the T-type calcium channel antagonist (30 μM nickel) failed to suppress calcium spikes (fraction of calcium-spike cells was 115% ± 41% of control, n = 2 slices, 536 cells, not shown). (2) The fraction of calcium-spike cells was not affected by blocking synaptic transmission using GABA$_A$-, AMPA-, and NMDA-receptor antagonists (antagonist cocktail #1: 10 μM bicuculline, 10 μM NBQX, 40 μM D-APV, 108% ± 16% of control, n = 11, Figure 3); subsequent addition of GABA$_B$ (5 μM CGP 55845), metabotropic glutamate (group I, 100 μM AIDA; group II/III, 100 μM CPPG), and muscarinic (10 μM

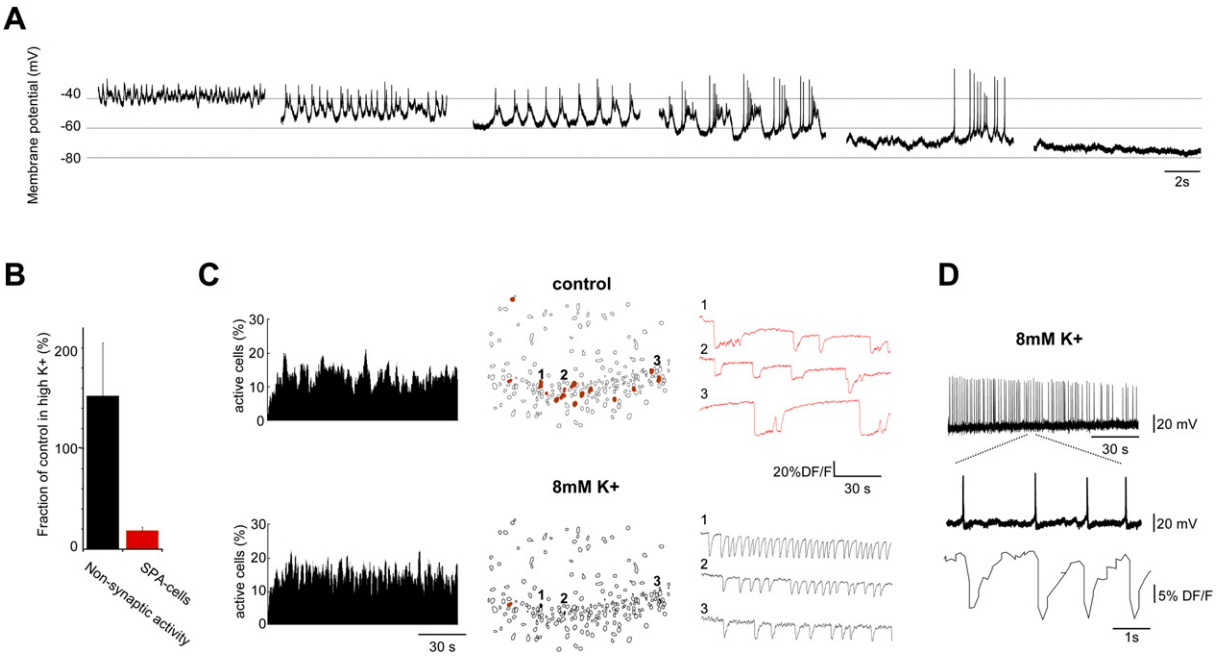

Figure 4. Voltage Dependence of the Membrane-Potential Fluctuations Produced during Calcium Plateaus

(A) Current-clamp recordings at different membrane potentials of a cell detected optically as producing calcium plateaus (SPAs). Note that the SPA activity is disturbed at potential values above −55 and below −65 mV. Cell was recorded at P3 in the presence of AMPA/kainate, NMDA, and $GABA_A$-R blockers.

(B) Bar histograms indicate the fraction of imaged cells detected as active at least once during the recording period (active cells [%]) in elevated potassium conditions (8 mM) relative to control conditions (i.e., in the presence of glutamate and $GABA_A$-R blockers). Black bar, fraction of intrinsically active cells, i.e., all cells active; red, fraction of active cells producing a calcium plateau (i.e., fraction of SPA cells). Error bars indicate SEMs.

(C) Histograms show the percentage of imaged cells that are detected as being active at each movie frame in control (same conditions as [B], top) and in 8 mM K+ (bottom). Red-filled contours in the maps of the imaged slice indicate SPA cells. Fluorescence traces show the calcium events in the three marked contours in both conditions. Note that all SPA cells stopped producing calcium plateaus in 8 mM K^+ (bottom).

(D) Simultaneous current-clamp recordings (Vrest ∼−60 mV, top traces) and calcium imaging (bottom trace) of spontaneous activity in high-potassium conditions and in the presence of glutamate and $GABA_A$-R blockers.

atropine) receptor antagonists also failed to block calcium spikes (fraction of calcium-spike cells in the presence of antagonist cocktail #2: 101% ± 7% of control, n = 4 slices, 902 cells, not shown).

SPAs are nonsynaptic voltage-gated events since (1) targeted current-clamp recordings from neurons producing SPAs revealed a strong voltage dependence of these events that were abolished when the cell was hyperpolarized (to Vm ∼−80 mV) or depolarized (to Vm ∼−40 mV; Figure 4). In keeping with this, raising—in the presence of ionotropic GABA- and glutamate-receptor antagonists—the extracellular potassium concentration from 3.5 to 8 mM to depolarize neurons (from −61 ± 1 mV to −44 ± 1 mV, respectively, n = 4 neurons) produced a highly significant drop of the fraction of active cells producing calcium plateaus, i.e., "fraction of SPA-cells" (to 26% ± 4% of control n = 5 slices, 1122 cells imaged, Figure 4, $p < 0.001$); (2) targeted whole-cell recordings showed that recurrent membrane-potential bursts were associated with sodium action potentials but also occurred in very immature neurons with poorly developed sodium conductances, suggesting that pure calcium currents could generate them. Accordingly, SPAs were sensitive to antagonists of L-type calcium and sodium channels (10 μM nifedipine and 1 μM TTX, reduction of the fraction of SPA cells to 6% ± 2% of control, n = 7 slices, 1476 cells, Figure 3), indicating that they were generated by high-threshold calcium currents with a contribution of sodium channels. (3) Like calcium spikes, the fraction of SPA cells was not affected by perfusion with antagonist cocktails #1 and #2 that included GABA, glutamate, and muscarinic receptor blockers (antagonist cocktail #2: 90% ± 12%, n = 4 slices, 902 cells). These cocktails also did not affect significantly the coherence between calcium plateaus (5.5% pairs of SPA cells correlated in blockers versus 7.8% pairs in control). In the presence of antagonist cocktail #1, we also performed voltage-clamp recordings from SPA cells (n = 3, Vh = −60 mV). In this condition, we did not observe any recurrent burst pattern in contrast to recordings performed in current-clamp mode (data not shown). Therefore, neither the generation nor the synchronization of SPAs was synapse-mediated. (4) Finally, we tested the involvement of Ih in the generation of SPA since this current is known to contribute significantly to the pacemaker

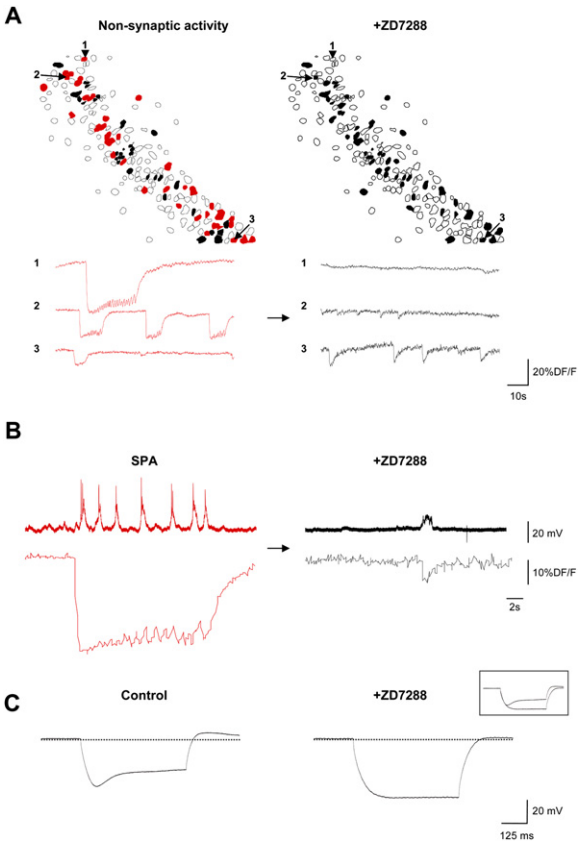

Figure 5. Role of Ih in the Generation of Calcium Plateaus

(A) All cells detected in control conditions (i.e., in the presence of AMPA/kainate, NMDA, and $GABA_A$-R blockers) as generating calcium plateaus (SPA cells, red-filled contours) only generated calcium spikes (calcium-spike cells, black-filled contours) when the specific blocker for the hyperpolarization-activated cationic current (ZD7288, 30 μM) was added to the saline. Traces below show the calcium fluorescence changes in the three cells indicated on the above contour maps.

(B) Simultaneous electrophysiological (current-clamp, Vrest ~−60 mV) and optical recording of an SPA cell in control (same conditions as [A]) and in the presence of ZD7288.

(C) The h-conductance activated by a hyperpolarizing step in control conditions in a neuron at birth (Vrest) is fully blocked in the presence of ZD7288.

mechanisms underlying rhythmic oscillations (Pape, 1996) and is functionally expressed in the hippocampus at early developmental stages (Brewster et al., 2006). The fraction of SPA cells was strongly reduced by ZD7288 (30 μM, to 14% ± 6% of control, n = 4 movies, 769 cells, Figure 5) or Cs (1 mM to 31% ± 4% of control, n = 3 movies, 571 cells). This effect was specific for SPAs since the fraction of calcium-spike cells was not affected by Ih blockade (94% ± 4% or 126% ± 8% of control in the presence of 30 μM ZD7288 or 1 mM Cs, respectively). Current-clamp recordings confirmed that SPA cells indeed expressed functional HCN channels as assessed by hyperpolarizing current injections (Figure 5), the blockade of which prevented recurrent membrane-potential oscillations and induced a slight hyperpolarization of the cell (~5 mV, Figure 5, n = 3). Interestingly, T-type calcium currents, also frequently involved in the generation of rhythmic oscillations (McCormick and Huguenard, 1992), were not contributing to SPAs, since the fraction of SPA cells was not affected by low concentrations of nickel (30 μM, to 125% ± 37% of control, n = 2 slices, 536 cells). In conclusion, calcium spikes and SPAs, the two early patterns of activity preceding the occurrence of GDPs, are mediated by intrinsic voltage-gated channels, Ih being specifically instrumental in generating SPAs but not calcium spikes. Since SPA cells represented the first neuronal ensemble operating as a network at a stage where most activity is intrinsic in isolated neurons, we next specifically examined the mechanisms controlling their synchronization.

SPAs Are Restricted to a Subnetwork of Gap Junction-Interconnected Neurons

Imaging of calcium dynamics clearly indicated that SPAs differ from calcium spikes and GDPs, not only by their unique kinetics but also by their being synchronized (unlike calcium spikes) and restricted to a small ensemble of neurons (unlike GDPs). Furthermore, such synchronization was robust, since coherence of activity among SPA cells persisted in the absence of synaptic transmission and since repeated synchronous activation of groups of SPA neurons could be observed (see for example Figure 8B). Since developing neurons are often connected by gap junctions (Bittman et al., 1997; Borodinsky et al., 2004; Corlew et al., 2004; Dupont et al., 2005; Lo Turco and Kriegstein, 1991; Owens and Kriegstein, 1998; Roerig and Feller, 2000; Sohl et al., 2005; Spitzer et al., 2004; Yuste et al., 1992), we tested the hypothesis that electrical synapses could selectively enable the generation of non-synaptic coherent SPAs in subnetworks of interconnected neurons. Bath applications of the specific gap-junction blockers mefloquine (Cruikshank et al., 2004) (25 μM, Figure 6) or carbenoxolone (100 μM) selectively blocked the occurrence of SPAs (fraction of SPA cells was 9% ± 4%, n = 6 slices and 26% ± 5%, n = 5 slices of control in the presence of mefloquine or carbenoxolone, respectively). This effect was specific for SPAs, since the fraction of calcium-spike cells was not affected by gap-junction blockers (75% ± 4% or 101% ± 27% of control in the presence of 25 μM mefloquine or 100 μM carbenoxolone, respectively). In keeping with this, we confirmed in a separate set of experiments by electrophysiological recordings that 25 μM mefloquine or 100 μM carbenoxolone did not affect calcium spikes (data not shown). As a result of blocking SPAs, correlated network activity dropped to the chance level observed for calcium spikes (0.52% pairs of SPA cells correlated in mefloquine, $p < 0.05$). In order to further establish the selective coupling by gap junctions between SPA cells, we injected intracellularly the coupling tracer neurobiotin or biocytin (Peinado et al., 1993) while imaging calcium activity in order to discriminate between

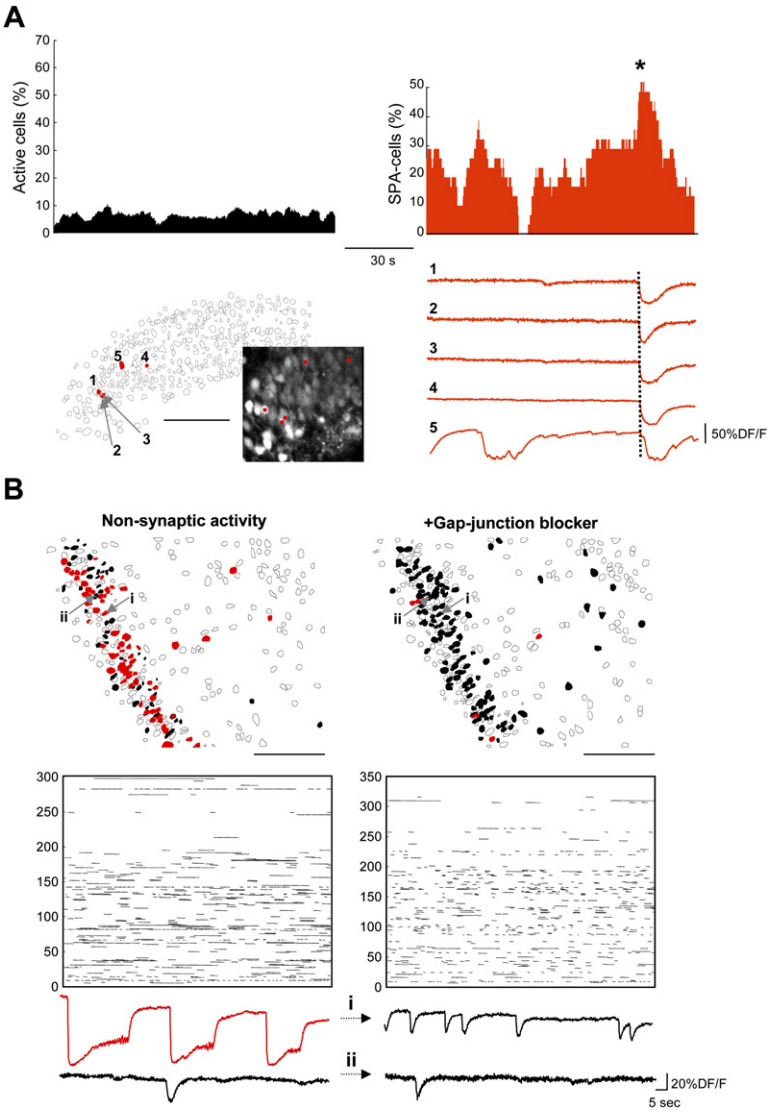

Figure 6. Calcium Plateaus Are Temporally Correlated and Selectively Affected by Gap Junction Blockers

(A) Representative histograms indicating the fraction of cells detected as being active for each movie frame relative to (left, black) the entire population of imaged cells and (right, red) to the subpopulation of SPA cells, i.e., cells producing characteristic calcium plateaus. Histograms show that early (illustrated example is P0) there is no emergent correlated activity but that the subpopulation of SPA cells synchronize their activity (asterisk). Lower-right fluorescence traces illustrate coactivation of five SPA cells (red-filled contours and red dots in the calcium fluorescence image).

(B) Representative example illustrating the effect of the gap-junction blocker mefloquine (25 μM) on nonsynaptic activity (i.e., in the presence of NBQX [10 μM], D-APV [40 μM], and bicuculline [10 μM]) at P2. Cells presenting calcium plateaus such as #i (arrow #i in the contour maps) are indicated by filled red contours whereas other intrinsically active cells such as #ii (arrow #ii in contour maps) are indicated by filled black contours. Mefloquine selectively affects calcium plateaus, as shown in the activity rasterplots and by the almost complete disappearance of filled red contours in the presence of the blocker (right panel) and by the changes in fluorescence traces between #i and #ii.

cells generating calcium spikes and SPAs. We found that neurobiotin or biocytin injection resulted in dye-labeling of clusters of neurons only in cells identified by imaging and electrophysiological recordings as generating SPA (100%, n = 7 cells recorded in seven slices, Figure S1, see also Figure 1B). In contrast, cells identified by imaging and electrophysiological recordings as generating calcium spikes but not SPAs, were not gap-junction connected to other neurons, as neurobiotin or biocytin injection resulted in dye-labeling of the recorded neuron only (in 12 out of 15 recorded cells from 15 slices, Figure S1). Therefore, SPAs are generated in cell assemblies that are gap-junction coupled in contrast to calcium spikes. We conclude that, during the perinatal period, a subnetwork of intrinsically active neurons assembles to generate, via gap-junction coupling, synchronized recurrent bursts that form the earliest endogenous pattern of correlated activity in the hippocampus. Because the maximum percentage of SPA cells was observed around birth, we next investigated whether SPAs could be regulated by delivery-associated mechanisms.

Delivery Triggers the Emergence of Population Coherence

We hypothesized that if parturition plays a role in the emergence of the first coherent pattern generated by the developing hippocampus, it should be regulated by signaling molecules involved in delivery. We therefore tested the effects of oxytocin (OT), an essential maternal hormone for labor induction (Gimpl and Fahrenholz, 2001). Treatment with oxytocin (1 μM) of slices from mice fetuses (E18) having been initially intracardially perfused with ACSF to wash out the endogeneous hormone caused a 3-fold increase in the fraction of SPA cells to levels comparable to birth stages (21% ± 2% of SPA cells at E18 in the presence of OT versus 9% ± 2% of SPA cells in control at E18,

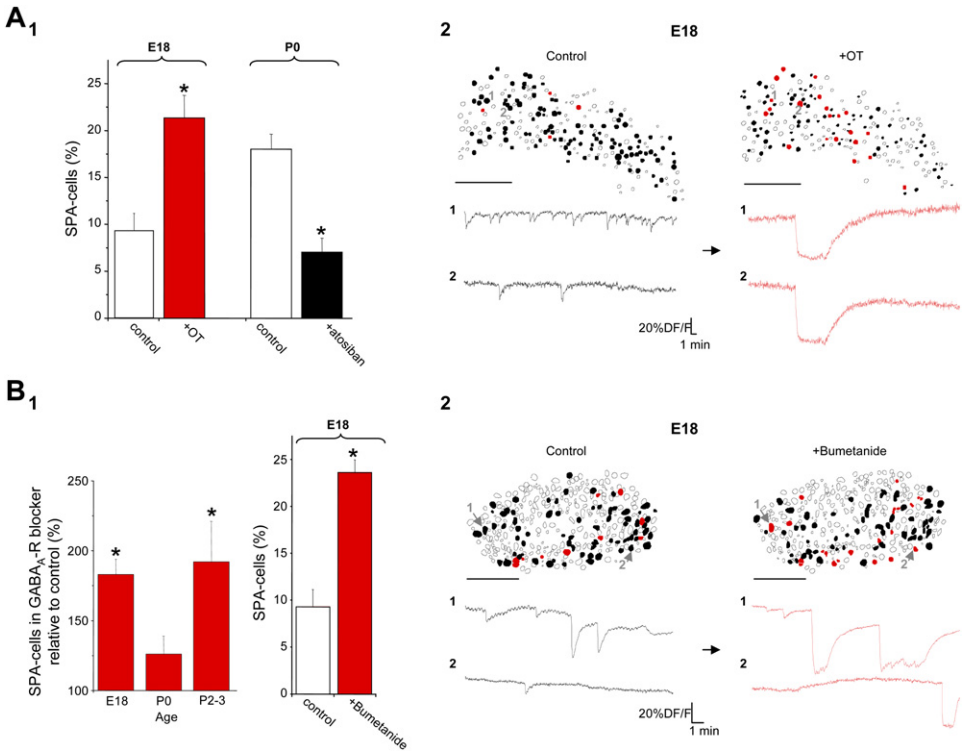

Figure 7. The Generation of Calcium Plateaus Is Regulated by Oxytocin

(A1) Histograms compare the averaged fraction of active cells producing a calcium plateau (fraction of SPA cells) at embryonic stages (E18) and at birth (P0) in control conditions (white bar), in the presence of oxytocin (OT 1 μM, red bar, n = 6 movies) and in the presence of the OT-receptor antagonist atosiban (1–5 μM, black bar, n = 8 movies). Error bars indicate SEMs, *p < 0.001. (A2) An important fraction of cells detected in control conditions as generating calcium spikes (black-filled contours) generate calcium plateaus (SPA cells, filled red contours) when OT is added to the saline, as shown in the illustrated contour map for a representative movie taken at embryonic stages (E18). Traces below show the calcium fluorescence changes in the two calcium-spike cells indicated on the above contour maps. They become SPA cells in the presence of OT.

(B1) Left histograms represent the fraction of SPA cells in the presence of the $GABA_A$-R blocker (bicuculline 10 μM) relative to control conditions (i.e., 10 μM NBQX and 40 μM D-APV). Note that the fraction of SPA cells is significantly boosted when blocking $GABA_A$-Rs at E18 and P2–P3 (*p < 0.05) while it remains unchanged at birth (P0, p > 0.05). Right histograms show that adding the selective NKCC1 antagonist bumetanide (10 μM, red bar) at embryonic stages (E18) selectively increases the fraction of SPA cells relative to the total number of active cells as compared to control conditions (white bar, *p < 0.01). Error bars indicate SEMs. (B2) An important fraction of cells detected in control conditions as generating calcium spikes (black-filled contours) generate calcium plateaus (SPA cells, filled red contours) when bumetanide (10 μM) is added to the saline, as shown in the illustrated contour maps for a representative movie taken at embryonic stages (E18). Traces below show the calcium fluorescence changes in the two neurons indicated in the above maps (1 and 2) that generate calcium spikes and that become SPA cells in the presence of bumetanide.

n = 15 movies, 5348 cells, p < 0.001, Figure 7). In contrast, the fraction of active cells relative to the total number of imaged neurons was not affected by the hormone (active cells: 45% ± 6% at E18 control versus 56% ± 4% at E18 in OT; n = 15 movies, 5348 cells, p > 0.05). Furthermore, intracardial perfusion of newborn mice, just at the time of delivery, with the selective oxytocin receptor antagonist atosiban (1 to 5 μM) prevented the emergence of SPA activity, since the fraction of SPA cells at birth in perfused slices dropped to levels comparable to embryonic stages (7% ± 1% of SPA cells at P0 in the presence of atosiban versus 18% ± 2% of SPA cells at P0 in control, n = 23 movies, 7147 cells, p < 0.001, Figure 7). In contrast, atosiban did not change the fraction of active cells relative to the total number of imaged neurons at P0 (active cells: 46% ± 6% at P0 control versus 52% ± 7% at P0 in atosiban; n = 23 movies, 7147 cells, p > 0.05). Therefore, we conclude that the emergence of SPAs is controlled by oxytocin and thus that it is a parturition-associated coherent activity pattern.

We next asked for the possible cellular mechanisms involved in the oxytocin-mediated enhancement of SPAs. Since oxytocin was recently shown to transiently convert GABA actions from excitatory to inhibitory by a downregulation of the NKCC1 chloride inward transporter activity (Tyzio et al., 2006), we hypothesized that the polarity of GABA actions could directly influence the occurrence of SPAs. We first investigated the near-term impact of $GABA_A$-receptor activation on the generation of SPA. We found that pharmacological blockade of $GABA_A$-Rs almost doubled the fraction of SPA cells relative to control conditions (NBQX 10 μM + D-APV 40 μM) both at

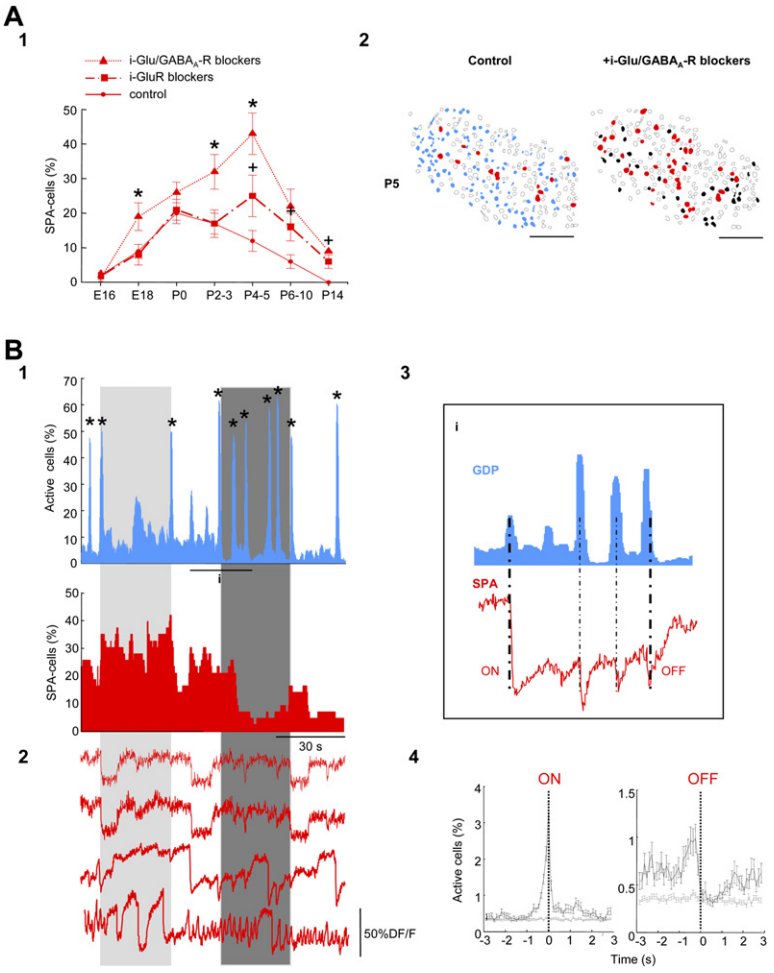

Figure 8. Modulation of SPAs by Synaptic Activities

(A1) Graph shows that the fraction of active cells producing a calcium plateau (SPA cells [%]) increases as synaptic activity is reduced by blockers of ionotropic glutamate receptors (10 μM NBQX, 40 μM D-APV) and when $GABA_A$ receptors are further blocked by bicuculline (10 μM) for the age groups E18 and P2–P10. +$p < 0.05$ when comparing fraction of SPA cells in control and glutamate-receptor blockers; *$p < 0.05$ when comparing fraction of SPA cells in glutamate-receptor blockers and glutamate- and $GABA_A$-receptor blockers. Error bars indicate SEMs. (A2) Representative contour maps of the effect of synaptic blockers on the distribution of SPA cells (filled red contours) on the same slice at a stage when GDPs dominate the network (P6). Blue-filled contours indicate cells that participate in GDPs without producing SPA. Black-filled contours indicate cells generating only calcium spikes. Scale bar, 100 μm.

(B1) SPA is anticorrelated with the occurrence of GDPs in the network, as shown by the histograms plotting the fraction of cells detected as being active for each movie frame relative to the entire population of imaged cells (top, blue) and to the subpopulation of SPA cells, i.e., cells producing characteristic calcium plateaus (bottom, red). Peaks in the number of coactive neurons in the blue histogram (*) correspond to GDPs. (B2) Calcium fluorescence changes in four SPA cells corresponding to the above recording. Note that the four SPA cells can participate to the GDP events. (B3) Expanded timescale of the activity recorded in (B1) and (B2). Histogram indicates GDPs and fluorescence trace the occurrence of a calcium plateau in an SPA cell. Bold dotted lines mark GDPs that turn ON/OFF the calcium plateau, whereas light dotted lines mark GDPs that do not affect the plateau (but that can be detected on the top of the plateau). (B4) Pooled data plot for 95 movies showing the fraction of active cells within a 6 s interval centered at the onset (left) and the offset (right) of calcium plateaus in control conditions (black) as well as in the presence of glutamate-receptor blockers (Experimental Procedures, gray). Error bars represent SEMs.

embryonic stages and a few days after birth (E18: 183% ± 11% of control, n = 5 slices, 1660 cells; P2–P3: 192% ± 29%, n = 7 slices, 2054 cells; $p < 0.05$, Figure 7, see also Figure 8) while it did not significantly affect the fraction of SPA cells at the time of delivery (P0: 126% ± 13% of control, n = 8 slices, 2672 cells). This suggested that GABA inhibits the emergence of SPAs when it has an excitatory action. Accordingly, we show that the application of the selective NKCC1 antagonist bumetanide (10 μM) at embryonic stages (E18) selectively increases the fraction of SPA cells (9% ± 2% SPA cells in control versus 23% ± 1% in bumetanide, n = 19 movies, 5303 cells, $p < 0.01$, Figure 7) without affecting the fraction of active cells in the network, thus reproducing the effects of oxytocin.

We conclude that the oxytocin-mediated transient inhibitory action of GABA occurring at birth favors the emergence of SPA.

SPAs and GDPs Are Temporally and Spatially Mutually Exclusive

Although SPAs and GDPs have different developmental profiles, they do coexist within the same neuronal network during the first postnatal week. To investigate their interactions, we first determined their precise developmental curves, then their spatiotemporal interactions.

We first calculated the fraction of SPA cells at E16 (n = 5 slices), E18–E19 (n = 15), P0–P2 (n = 20), P3–P5 (n = 14), P6–P10 (n = 13), and P14 (n = 6). We found that the developmental decline of SPAs, which started at P0–P2, was clearly anticorrelated with the progressive expansion of GDPs that peaked at P6–P10 (Figure 2). Since GABAergic and glutamatergic synapses, which mediate GDPs, mature progressively during the same period, we determined the effects of blocking GABA and/or glutamate synapses on the developmental expression of SPAs. We found

that blocking both $GABA_A$ and glutamate ionotropic receptors restored SPAs during the first postnatal week, but not after P14 (or before E19, Figure 8), suggesting that synapse-driven events inhibit the expression of SPAs. Interestingly, in keeping with the earlier maturation of GABAergic transmission (Ben Ari, 2001), blockade of glutamate receptors alone failed to increase significantly the fraction of SPA cells at birth (P0–P2) but efficiently rescued the fraction of SPA cells starting from P3–P5 (Figure 8). These results suggest that GABA-driven then glutamate-driven synaptic events can switch off SPAs in keeping with their maturation gradients. They also suggest that the critical period during which the immature network is capable of returning to gap-junction-synchronized calcium plateaus ends around the second postnatal week.

When GDPs and SPAs coexist within the hippocampal network (P3–P7), they are mutually exclusive. We marked the onset and offset of each calcium plateau (SPA) and averaged activity time-locked to these two time references. SPAs were strongly regulated by the occurrence of GDPs in a temporal and spatial manner. We observed a significant peak of network synchrony at the onset and just before the offset of SPAs (Figure 8). Both peaks of synchrony corresponded to the occurrence of a GDP since they were blocked when synaptic transmission was suppressed. Results indicated that SPAs tended to turn ON at GDP offset and turn OFF at the onset of a subsequent GDP (Figure 8). In addition, since we could localize neurons involved in any given GDP, we compared the spatial distribution of GDP events that turned OFF SPAs to GDPs that did not alter SPAs. Most SPA cells, besides from generating calcium plateaus, also participated to GDPs (see examples in Figure 8B). Moreover, we found that, on average, a GDP that shut off a calcium plateau involved more cells within a 20 μm radius from the cell generating an SPA than an ineffective one (24% ± 3% neurons versus 14% ± 0.7% $p < 0.05$). Therefore, GDPs effectively influence the generation of SPAs when they occur in their vicinity. We propose that the synaptic influx during a GDP interferes with SPAs by switching them OFF.

DISCUSSION

The combined use of fast multibeam two-photon imaging to analyze calcium dynamics from hundreds of neurons and of targeted electrophysiological recordings has enabled us to follow a cascade of three patterns representing the transition from an ensemble of neurons at embryonic stages (E16) endowed with sparse and uncorrelated activities to a neuronal network communicating by means of thousands of synapses and generating the massively synchronized GDPs (P5–P10). To our knowledge, this is the first time that the dynamics of three distinct spontaneous activity patterns are followed simultaneously from embryo to juvenile stages within the same cortical network. We propose that the emergence of population coherence in the CA1 hippocampus is controlled by the physiological changes taking place during delivery and disappears when the synaptic circuitry is capable of generating GDPs. Since excellent reviews of the maturation of retinal waves (Firth et al., 2005) and spinal cord oscillations (Spitzer et al., 2004) are available, we shall restrict our discussion to cortical structures.

Cellular Mechanisms for the Generation of SPAs

At embryonic stages, hippocampal neurons generate fast intrinsic calcium events (mean duration < 3 s) that do not propagate to other neurons. These events seem to occur randomly, on average twice a minute, with no intercellular synchrony. Current-clamp recordings indicated that they corresponded to spontaneous calcium spikes. Since they occurred in only 10% of cells at E16, they are most likely the first sign of electrical activity of the immature hippocampus. These primitive calcium spikes seem to indistinctively concern all neuronal types in the network. Similar single-cell calcium events have been reported in the ventricular zone at late embryonic stages (Owens and Kriegstein, 1998; Weissman et al., 2004) and in spinal neurons (Gu and Spitzer, 1995; Gu and Spitzer, 1997), although less frequent and with ten times longer kinetics. Furthermore, calcium fluctuations in cortical precursor cells do not involve voltage-gated calcium channels in contrast to these spikes that required both sodium and calcium voltage-gated conductances for their generation. A strong contribution of L-type calcium channels to their generation is indicated by the fact that the L-type antagonist nifedipine abolished almost all calcium activity before birth. Interestingly, a similar critical role for L-type channels at early developmental stages has been reported in other structures (Corlew et al., 2004; Liljelund et al., 2000; Singer et al., 2001). Neither gap junctions nor transmitter-gated channels are involved in the generation of these sporadic individual events, since they are resistant to both ligand-gated channels and gap-junction antagonists.

A discrete group of neurons (around 20% of active cells) later coassemble and generate synchronized calcium plateaus nesting recurrent membrane-potential oscillations. Although both SPAs and calcium spikes involve sodium and calcium voltage-gated conductances and are neither synapse-driven nor metabotropic-receptor dependent, they are generated by different mechanisms. In contrast to calcium spikes, SPAs require the activation of the hyperpolarization-activated cationic current Ih, since they were fully and selectively blocked by ZD7288 or external Cs. Immunohistochemical studies indicate that several HCN isoforms (in particular HCN-4) are already expressed at birth in the CA1 region (Brewster et al., 2006; Vasilyev and Barish, 2002). An upregulation of Ih at birth mirroring the emergence of SPAs has been described in phrenic motoneurons (Di et al., 2001). We confirm that an H-conductance can be activated in hippocampal neurons at this stage. Interestingly, there is a transient hyperpolarization of the resting membrane potential of hippocampal neurons at birth (Tyzio et al., 2003, 2006) that should facilitate the activation of Ih and the generation of oscillatory activity. Ih is instrumental in the generation of many central

patterns that occur within the same frequency range (<1 Hz) (Bender et al., 2005; Blethyn et al., 2006; Nita et al., 2003; Pape and McCormick, 1989). The generation of SPAs is also conditioned by gap-junction coupling between a restricted assembly of intrinsically active neurons since (1) blockade of gap junctions selectively prevents the occurrence of calcium plateaus without affecting the electrical properties of neurons, including the generation of voltage-gated calcium currents (data not shown) or of calcium spikes. (2) Intracellular dye injection from targeted cells producing SPAs resulted in the labeling of cell clusters, whereas similar experiments in neurons producing calcium spikes resulted in single-cell labeling. It remains to be determined how electrical coupling can produce membrane potential recurrent oscillations (Leznik and Llinas, 2005). It is a complex issue since it concerns the mechanisms for an emergent network property, and modeling studies should help provide some clues (Loewenstein et al., 2001).

There is an abundant literature on the early maturation of gap junctions and the importance of intracellular coupling as a communication system in developing structures in various animal species (Rozental et al., 2000). Gap-junction coupling supports biochemical communication (Kandler and Katz, 1998; Yuste et al., 1992, 1995), mediates the spread of membrane depolarization or of calcium signals (Corlew et al., 2004; Dupont et al., 2005; Katz and Shatz, 1996; Liljelund et al., 2000; Lo Turco and Kriegstein, 1991; Owens and Kriegstein, 1998; Singer et al., 2001), and may influence the cellular expression of the conductances mediating Ih (Schulz et al., 2006). It is worth stressing that, in contrast to earlier studies (Corlew et al., 2004; Dupont et al., 2005), pharmacological blockade of gap junctions selectively blocks synchronization-dependent events (SPAs), whereas ongoing intrinsic calcium spikes are not affected. This and other observations suggest that SPAs and earlier intrinsic calcium spikes coexist during a transitional period. Therefore, at embryonic stages, neurons first fire calcium spikes individually before interconnecting via gap junctions at birth to generate the first coherent pattern of activity (SPA).

SPA: A Specific Coherent Pattern Synchronizing Small Cell Assemblies

SPAs correspond to the synchronous activation of discrete neuronal assemblies that remain coactive for several seconds. Although they share some features with other immature cortical activities (vide supra), they are different from GDPs (Leinekugel et al., 1998), early network oscillations (Corlew et al., 2004; Garaschuk et al., 2000; McCabe et al., 2006; Meister et al., 1991), cholinergic cortical oscillations (Dupont et al., 2005; Peinado, 2000), intracellular calcium fluctuations in precursor cells (Owens and Kriegstein, 1998), or cortical domains (Kandler and Katz, 1998; Yuste et al., 1992) since:

(1) SPAs have unique calcium dynamics with fast onset kinetics lasting less than 200 ms. The kinetics of the calcium plateaus is slow and results in a robust and sustained calcium influx as opposed to synapse-driven early network events (Garaschuk et al., 2000; Leinekugel et al., 1997). The duration of the plateau is comparable to that of the spontaneous calcium fluctuations reported in the ventricular zone (Owens and Kriegstein, 1998) or in cultured Purkinje neurons (Liljelund et al., 2000). The temporal structure of the membrane-potential fluctuations occurring during SPAs is also remarkable, since SPA neurons oscillate relatively fast (at around 0.5 Hz), suggesting they might represent a pacemaker ensemble. The comparison with earlier studies performed in immature cortical structures regarding this point is difficult, since most of these investigations focused on calcium activity, sometimes associated to field-potential recordings (Corlew et al., 2004; Dupont et al., 2005; Garaschuk et al., 2000), but only very few have performed single-cell electrophysiological recordings to identify the underlying physiological events while imaging (Leinekugel et al., 1997; Liljelund et al., 2000; Peinado, 2000).

(2) SPAs are nonsynaptic events that are not blocked by antagonists of ligand-gated channels in contrast to cortical oscillations (Dupont et al., 2005; Garaschuk et al., 2000; McCabe et al., 2006; Peinado, 2000).

(3) SPAs are blocked by global neuronal depolarization in elevated extracellular potassium conditions as opposed to many coherent immature activities (Corlew et al., 2004; Garaschuk et al., 2000; Sipila et al., 2005; Yuste et al., 1992). This and other observations indicate that the generation of SPAs is mediated by voltage-gated signaling with no intervention of synaptic currents.

(4) SPAs are confined spatially and temporally to a restricted population of neurons. They do not propagate, thus resembling a "chord" (see Movie S1) rather than a "wave" (see Movie S2). Their temporal and spatial confinement to a small cell assembly coupled by gap junctions suggests a sort of syncytium generating calcium plateaus. In that respect, they can be compared to cortical domains (Owens and Kriegstein, 1998; Yuste et al., 1995) but differ from other reported cortical waves that propagate to the entire cortical mantle (Dupont et al., 2005). They also have a more restricted spatial coherence than most immature neuronal patterns that also synchronize large groups of neighboring neurons (Bittman et al., 1997; Garaschuk et al., 2000; Leinekugel et al., 1997; Wong et al., 1993).

Possible Significance of the Developmental Curve of Expression of SPAs

The three developmental curves described here clearly provide a signature for the different coherent electrical

activity patterns prevailing at three developmental stages: embryonic, parturition, and postnatal. Our results show that SPAs present a unique bell-shaped developmental profile centered at birth. Interestingly, other coherent activity patterns with a frequency peaking around birth have been previously described in immature cortical structures (Corlew et al., 2004; Garaschuk et al., 2000). We provide here evidence that, in the hippocampus, delivery actually phases the emergence of population coherence. Indeed, we show that the shift from individual calcium spikes to SPAs is raised by maternal hormones released during delivery. Thus, early oxytocin application to fetuses shifted the peak of the developmental curve for the emergence of SPAs to embryonic stages, whereas birth application of the selective oxytocin-receptor antagonist on the contrary delayed the expression of SPAs. Oxytocin was shown to exert multiple effects in the nervous system (Argiolas and Gessa, 1991; Raggenbass, 2001; Theodosis et al., 2006; Tomizawa et al., 2003). In particular, during delivery, maternal oxytocin triggers major changes in fetal neurons by modulating intracellular chloride concentration via a downregulation of the KCC1 transporter activity acting directly on oxytocin receptors (Tyzio et al., 2006). We show that the same pathways involved in the oxytocin-mediated transient shift of the actions of GABA from excitation to inhibition (Tyzio et al., 2006) also control the emergence of SPAs at birth. Several mechanisms could explain such enhancement of intrinsic calcium plateaus. For example, a hyperpolarizing action of GABA may favor the activation of Ih or create suitable and stable membrane-potential conditions for the generation of voltage-dependent membrane-potential oscillations. Besides, since a depolarizing GABA action increased intracellular calcium levels (Tyzio et al., 2006) and given that gap-junction coupling is negatively modulated by calcium (Arumugam et al., 2005; Connors and Long, 2004), another possibility could be that oxytocin indirectly favors SPAs via an action on gap junctions. A G protein signaling cascade involving cyclic nucleotide-dependent pathways (Gimpl and Fahrenholz, 2001) could also be involved, given their positive modulation of gap-junction coupling (Connors and Long, 2004; Hatton and Yang, 1996).

Finally, our imaging approach has enabled a comparison of three patterns that cohabitate after birth: SPAs and GDPs. We found a strong ON/OFF relationship between SPAs and GDPs. Indeed, we show that GDPs synchronize both a neuronal network operating through synaptic connections and, at their offset, subnetworks of immature neurons producing SPAs. Therefore, GDPs constitute another synchronizing mechanism for calcium plateaus that may reinforce the specificity of the calcium message associated with SPAs and perhaps provide a signal for shutting them off through synaptic currents. Several mechanisms could underlie the functional "inhibition" of SPAs by GDPs. It is possible that the strong depolarization of the membrane potential during GDPs directly affects the stability of voltage-dependent membrane oscillations as revealed by the sensitivity of SPAs to membrane potential during recordings. In the long range, activation of NMDA receptors during GDPs (Leinekugel et al., 1997) could produce a downregulation of connexin expression as previously established in hypothalamic neurons (Arumugam et al., 2005).

Conclusions and Possible Functions of SPAs

Using fast dynamic calcium imaging, we found an intermediate step in the maturation of network activities emerging at birth and during which small neuronal assemblies generate calcium plateaus nesting membrane-potential bursts (SPAs). Several observations suggest that sustained elevations of intracellular calcium concentration at preferential frequencies encode a specific trigger signal to pathways regulating gene transcription (Dolmetsch et al., 1997; Gu and Spitzer, 1995). We thus propose that the calcium plateaus associated with SPAs provide a specific signal for phenotypic or other functional specifications through the activation of a set of genes (Borodinsky et al., 2004; Gu and Spitzer, 1995; Jiang and Swann, 2005; Redmond and Ghosh, 2005; Sohl et al., 2005; Spitzer et al., 2004) or induce the diffusion of a messenger molecule between the cells making up this inaugural microcircuit. SPAs could thus provide a mechanism to reinforce the initial sorting of phenotypes according to their spatiotemporal origins (Butt et al., 2005). The assemblies of neurons formed may constitute an early form of functional unit preceding the organization by synaptic activity of cortical columns and other types of functional entities (Donoghue and Rakic, 1999).

EXPERIMENTAL PROCEDURES

Slice Preparation and Two-Photon Imaging

Transverse hippocampal slices (300 μm thick) were prepared from E16 to 14-day-old (P15) Swiss mice, using a Microm tissue slicer (International GmbH, Germany) with ice-cold oxygenated modified artificial cerebrospinal fluid (mACSF), with 0.5 mM $CaCl_2$ and 7 mM $MgSO_4$, and in which NaCl was replaced by an equimolar concentration of choline. Slices were then transferred for rest (around 1 hr) in oxygenated normal ACSF containing (in mM): 126 NaCl, 3.5 KCl, 1.2 NaH_2PO_4, 26 $NaHCO_3$, 1.3 $MgCl_2$, 2.0 $CaCl_2$, and 10 D-glucose, pH 7.4. For AM-loading, slices were incubated in a small vial containing 2.5 ml of oxygenated ACSF with 25 μl of a 1 mM Fura2-a.m. solution (Molecular Probes; in 100% DMSO) for 20–30 min. Slices were incubated in the dark, and the incubation solution was maintained at 35°C–37°C. Experiments were performed at 30°C–32°C with normal ACSF and continuously aerated with 95% O_2/5% CO_2. Imaging was performed with a multibeam two-photon laser scanning system (Trimscope-LaVision Biotec, Germany) coupled to an Olympus microscope. This system is based on a patented beamsplitter that splits up the incoming femtosecond laser beam (provided by a Ti:Sapphire laser source, Chameleon, Coherent, USA, excitation wavelength: 780 nm) into 64 beamlets, which are scanned simultaneously (scan rate 1 KHz) in the slice. This results in 64 times higher image acquisition rates compared to conventional multiphoton scanning microscopes. Images were acquired through a CCD camera (La Vision Imager 3QE), which typically resulted in a time resolution of 100 ms for full frames corresponding to the readout time of the camera. Slices were imaged using a low-magnification, high numerical aperture objective (20×, NA-0.95, Olympus). The size of the imaged field was typically ~430 × 380 μm^2 ; 2 × 2 binning, pixel size: 600 nm.

Pharmacology

Antagonists for $GABA_A$ and glutamate receptors mentioned in the manuscript are bicuculline (10 μM), NBQX (10 μM), and D-APV (40 μM). All drugs except TTX (Tocris) were purchased from Sigma.

Electrophysiology

Cells were held in current clamp using a patch-clamp amplifier (HEKA, EPC10). Pipette solution contained 130 mM $KMethylSO_4$, 5 mM KCl, 5 mM NaCl, 10 mM HEPES, 2.5 mM Mg-ATP, 0.3 mM GTP, 30 μM of Fura-2 pentapotassium salt (Molecular Probes), and 0.5% biocytin or 0.5% neurobiotin for post hoc reconstruction of recorded neurons and identification of cells interconnected via gap junctions. The osmolarity was 265–275 mOsm, pH 7.3. Microelectrodes had a resistance of 4–8 MΩ. Recordings were digitized online (20 kHz) with a Labmaster interface card (Molecular Devices) to a personal computer and acquired using Axoscope 7.0 software (Molecular Devices). To exclude possible interference with the calcium dye, neurons at P0–P1 were also patch clamped blindly (n = 23) without dye loading. In these conditions, we found that 22% of neurons displayed spontaneous recurrent burst discharges (DV = 16 ± 3 mV, n = 5 cells, data not shown) when neurons where recorded at resting membrane potential (−64 ± 1 mV, n = 5 cells).

Analysis

Analysis was performed with custom-made software in Matlab (MathWorks, Natick, MA). We developed a program aimed at the automatic identification of loaded hippocampal cells and at measuring their fluorescence as a function of time. This program is an improved version of the previously designed software for cortical slice analysis (Cossart et al., 2003). We encountered two major problems for an automatic identification of cells in an image: (1) variations in background fluorescence, which precluded the use of a uniform threshold value throughout the image and (2) the inability of a simple thresholding procedure to separate nearby cells. The latter problem was especially severe in the dense pyramidal cell layer of the hippocampus. As before (Cossart et al., 2003), we solved the problem of background variations by normalizing each pixel by the average fluorescence in its vicinity. We also convolved the image with a two-dimensional Gaussian (σ = 6 μm), which emphasized circular neuronal shapes and partially separated nearby neurons. A threshold (usually top 10 percentile of the overall pixel fluorescence distribution) was applied to the image to separate cell contours from the background. In order to complete the separation of nearby cells, we measured a circularity threshold for every contour, defined as $c = P^2/(4A)$, where P is the perimeter and A is the area of a contour. High values of c (usually >4) identified highly noncircular shapes usually indicative on unseparated cell contours. Local fluorescence maxima were identified within such contours, and the contours were separated into a corresponding number of concave shapes. All image processing was performed on time averages of recorded movies. The calcium signal of each cell was the average fluorescence within the contour of that cell, measured as a function of time. The analysis was performed separately for each hippocampal layer, with the borders between layers drawn manually. The entire procedure could be performed online sufficiently quickly to identify cells for targeted patch-clamp recordings. Signal-processing algorithms of MiniAnalysis software (Synaptosoft, Decatur, GA) were used to detect the onsets and offsets (time of half-amplitude decay) of calcium signals within the traces of individual cells. Active cells are neurons exhibiting at least one calcium event within the period of recording.

To compute the activity correlation of two cells, the onset of each event was represented by a Gaussian (σ = 1 frame, to allow some jitter). The inner product of the resulting values was then calculated. The significance of each correlation value was estimated by direct comparison with a distribution computed from surrogate data sets, in which the events were randomly reshuffled in time.

To discriminate between calcium plateaus (SPAs), and calcium transients (calcium spikes or GDPs), we visually sorted these activities based on the presence or absence of a calcium plateau. The characteristic feature of a calcium plateau is that it sustains a calcium level for several frames as opposed to a calcium spike, which starts decaying at the peak. We therefore considered that all events that stayed within ~5% of their peak amplitude for more than ~500 ms corresponded to calcium plateaus. Whereas SPAs had a clear plateau followed by decay, calcium spikes and GDPs had the decay in calcium fluorescence immediately following the increase (Figure 2). Manual analysis was done blindly to the experimental condition. We also performed a fully automated analysis of a sample of our data with criteria similar to that used for visual inspection: calcium plateaus are events with a peak amplitude of 20% DF/F persisting for at least 30 frames (>4 s). Such automated analysis gave typical errors of less than 3% from manual analysis (n = 12 movies reanalyzed).

Supplemental Data

The Supplemental Data for this article can be found online at http://www.neuron.org/cgi/content/full/54/1/105/DC1/.

ACKNOWLEDGMENTS

We thank Drs. Y. Buzsaki, J. Epsztein, R. Khazipov, R. Tyzio, F. Michel, and C. Hammond for critical comments. This work was supported by grants from the INSERM, the Ville de Marseille and Region P.A.C.A., the F.R.M and the F.R.C. Drs. R.C. and A.R. are funded by the CNRS.

Received: February 7, 2006
Revised: January 25, 2007
Accepted: March 9, 2007
Published: April 4, 2007

REFERENCE

Argiolas, A., and Gessa, G.L. (1991). Central functions of oxytocin. Neurosci. Biobehav. Rev. *15*, 217–231.

Arumugam, H., Liu, X., Colombo, P.J., Corriveau, R.A., and Belousov, A.B. (2005). NMDA receptors regulate developmental gap junction uncoupling via CREB signaling. Nat. Neurosci. *8*, 1720–1726.

Ben Ari, Y. (2001). Developing networks play a similar melody. Trends Neurosci. *24*, 353–360.

Ben Ari, Y. (2002). Excitatory actions of gaba during development: the nature of the nurture. Nat. Rev. Neurosci. *3*, 728–739.

Ben Ari, Y., Cherubini, E., Corradetti, R., and Gaiarsa, J.L. (1989). Giant synaptic potentials in immature rat CA3 hippocampal neurones. J. Physiol. *416*, 303–325.

Bender, R.A., Galindo, R., Mameli, M., Gonzalez-Vega, R., Valenzuela, C.F., and Baram, T.Z. (2005). Synchronized network activity in developing rat hippocampus involves regional hyperpolarization-activated cyclic nucleotide-gated (HCN) channel function. Eur. J. Neurosci. *22*, 2669–2674.

Bittman, K., Owens, D.F., Kriegstein, A.R., and LoTurco, J.J. (1997). Cell coupling and uncoupling in the ventricular zone of developing neocortex. J. Neurosci. *17*, 7037–7044.

Blethyn, K.L., Hughes, S.W., Toth, T.I., Cope, D.W., and Crunelli, V. (2006). Neuronal basis of the slow (<1Hz) oscillation in neurons of the nucleus reticularis thalami in vitro. J. Neurosci. *26*, 2474–2486.

Borodinsky, L.N., Root, C.M., Cronin, J.A., Sann, S.B., Gu, X., and Spitzer, N.C. (2004). Activity-dependent homeostatic specification of transmitter expression in embryonic neurons. Nature *429*, 523–530.

Brewster, A.L., Chen, Y., Bender, R.A., Yeh, A., Shigemoto, R., and Baram, T.Z. (2006). Quantitative analysis and subcellular distribution of mRNA and protein expression of the hyperpolarization-activated cyclic nucleotide-gated channels throughout development in rat hippocampus. Cereb. Cortex *17*, 702–712.

Butt, S.J., Fuccillo, M., Nery, S., Noctor, S., Kriegstein, A., Corbin, J.G., and Fishell, G. (2005). The temporal and spatial origins of cortical interneurons predict their physiological subtype. Neuron *48*, 591–604.

Cang, J., Renteria, R.C., Kaneko, M., Liu, X., Copenhagen, D.R., and Stryker, M.P. (2005). Development of precise maps in visual cortex requires patterned spontaneous activity in the retina. Neuron *48*, 797–809.

Colin-Le Brun, I., Ferrand, N., Caillard, O., Tosetti, P., Ben Ari, Y., and Gaiarsa, J.L. (2004). Spontaneous synaptic activity is required for the formation of functional GABAergic synapses in the developing rat hippocampus. J. Physiol. *559*, 129–139.

Connors, B.W., and Long, M.A. (2004). Electrical synapses in the mammalian brain. Annu. Rev. Neurosci. *27*, 393–418.

Corlew, R., Bosma, M.M., and Moody, W.J. (2004). Spontaneous, synchronous electrical activity in neonatal mouse cortical neurones. J. Physiol. *560*, 377–390.

Cossart, R., Aronov, D., and Yuste, R. (2003). Attractor dynamics of network UP states in the neocortex. Nature *423*, 283–288.

Cossart, R., Ikegaya, Y., and Yuste, R. (2005). Calcium imaging of cortical networks dynamics. Cell Calcium *37*, 451–457.

Cruikshank, S.J., Hopperstad, M., Younger, M., Connors, B.W., Spray, D.C., and Srinivas, M. (2004). Potent block of Cx36 and Cx50 gap junction channels by mefloquine. Proc. Natl. Acad. Sci. USA *101*, 12364–12369.

Di, P.E., Tell, F., Ptak, K., Monteau, R., and Hilaire, G. (2001). Perinatal changes of I(h) in phrenic motoneurons. Eur. J. Neurosci. *13*, 1403–1410.

Dolmetsch, R.E., Lewis, R.S., Goodnow, C.C., and Healy, J.I. (1997). Differential activation of transcription factors induced by Ca2+ response amplitude and duration. Nature *386*, 855–858.

Donoghue, M.J., and Rakic, P. (1999). Molecular gradients and compartments in the embryonic primate cerebral cortex. Cereb. Cortex *9*, 586–600.

Dupont, E., Hanganu, I.L., Kilb, W., Hirsch, S., and Luhmann, H.J. (2005). Rapid developmental switch in the mechanisms driving early cortical columnar networks. Nature *439*, 79–83.

Firth, S.I., Wang, C.T., and Feller, M.B. (2005). Retinal waves: mechanisms and function in visual system development. Cell Calcium *37*, 425–432.

Galli, L., and Maffei, L. (1988). Spontaneous impulse activity of rat retinal ganglion cells in prenatal life. Science *242*, 90–91.

Garaschuk, O., Linn, J., Eilers, J., and Konnerth, A. (2000). Large-scale oscillatory calcium waves in the immature cortex. Nat. Neurosci. *3*, 452–459.

Gimpl, G., and Fahrenholz, F. (2001). The oxytocin receptor system: structure, function, and regulation. Physiol. Rev. *81*, 629–683.

Gu, X., and Spitzer, N.C. (1995). Distinct aspects of neuronal differentiation encoded by frequency of spontaneous Ca2+ transients. Nature *375*, 784–787.

Gu, X., and Spitzer, N.C. (1997). Breaking the code: regulation of neuronal differentiation by spontaneous calcium transients. Dev. Neurosci. *19*, 33–41.

Hatton, G.I., and Yang, Q.Z. (1996). Synaptically released histamine increases dye coupling among vasopressinergic neurons of the supraoptic nucleus: mediation by H1 receptors and cyclic nucleotides. J. Neurosci. *16*, 123–129.

Jiang, M., and Swann, J.W. (2005). A role for L-type calcium channels in the maturation of parvalbumin-containing hippocampal interneurons. Neuroscience *135*, 839–850.

Kandler, K., and Katz, L.C. (1998). Coordination of neuronal activity in developing visual cortex by gap junction-mediated biochemical communication. J. Neurosci. *18*, 1419–1427.

Kandler, K., and Gillespie, D.C. (2005). Developmental refinement of inhibitory sound-localization circuits. Trends Neurosci. *28*, 290–296.

Kasyanov, A.M., Safiulina, V.F., Voronin, L.L., and Cherubini, E. (2004). GABA-mediated giant depolarizing potentials as coincidence detectors for enhancing synaptic efficacy in the developing hippocampus. Proc. Natl. Acad. Sci. USA *101*, 3967–3972.

Katz, L.C., and Shatz, C.J. (1996). Synaptic activity and the construction of cortical circuits. Science *274*, 1133–1138.

Khazipov, R., Esclapez, M., Caillard, O., Bernard, C., Khalilov, I., Tyzio, R., Hirsch, J., Dzhala, V., Berger, B., and Ben Ari, Y. (2001). Early development of neuronal activity in the primate hippocampus in utero. J. Neurosci. *21*, 9770–9781.

Khazipov, R., Sirota, A., Leinekugel, X., Holmes, G.L., Ben Ari, Y., and Buzsaki, G. (2004). Early motor activity drives spindle bursts in the developing somatosensory cortex. Nature *432*, 758–761.

Leinekugel, X., Khalilov, I., Ben Ari, Y., and Khazipov, R. (1998). Giant depolarizing potentials: the septal pole of the hippocampus paces the activity of the developing intact septohippocampal complex in vitro. J. Neurosci. *18*, 6349–6357.

Leinekugel, X., Medina, I., Khalilov, I., Ben Ari, Y., and Khazipov, R. (1997). Ca2+ oscillations mediated by the synergistic excitatory actions of GABA(A) and NMDA receptors in the neonatal hippocampus. Neuron *18*, 243–255.

Leznik, E., and Llinas, R. (2005). Role of gap junctions in synchronized neuronal oscillations in the inferior olive. J. Neurophysiol. *94*, 2447–2456.

Liljelund, P., Netzeband, J.G., and Gruol, D.L. (2000). L-Type calcium channels mediate calcium oscillations in early postnatal Purkinje neurons. J. Neurosci. *20*, 7394–7403.

Lo Turco, J.J., and Kriegstein, A.R. (1991). Clusters of coupled neuroblasts in embryonic neocortex. Science *252*, 563–566.

Loewenstein, Y., Yarom, Y., and Sompolinsky, H. (2001). The generation of oscillations in networks of electrically coupled cells. Proc. Natl. Acad. Sci. USA *98*, 8095–8100.

Malek, A., Blann, E., and Mattison, D.R. (1996). Human placental transport of oxytocin. J. Matern. Fetal Med. *5*, 245–255.

McCabe, A.K., Chisholm, S.L., Picken-Bahrey, H.P., and Moody, W.J. (2006). The self-regulating nature of spontaneous synchronized activity in developing mouse cortical neurones. J. Physiol. *577*, 155–167.

McCormick, D.A., and Huguenard, J.R. (1992). A model of the electrophysiological properties of thalamocortical relay neurons. J. Neurophysiol. *68*, 1384–1400.

Meister, M., Wong, R.O., Baylor, D.A., and Shatz, C.J. (1991). Synchronous bursts of action potentials in ganglion cells of the developing mammalian retina. Science *252*, 939–943.

Nielsen, T., Fricke, M., Hellweg, D., and Andresen, P. (2001). High efficiency beam splitter for multifocal multiphoton microscopy. J. Microsc. *201*, 368–376.

Nita, D.A., Steriade, M., and Amzica, F. (2003). Hyperpolarisation rectification in cat lateral geniculate neurons modulated by intact corticothalamic projections. J. Physiol. *552*, 325–332.

O'Donovan, M.J. (1989). Motor activity in the isolated spinal cord of the chick embryo: synaptic drive and firing pattern of single motoneurons. J. Neurosci. *9*, 943–958.

Owens, D.F., and Kriegstein, A.R. (1998). Patterns of intracellular calcium fluctuation in precursor cells of the neocortical ventricular zone. J. Neurosci. *18*, 5374–5388.

Palva, J.M., Lamsa, K., Lauri, S.E., Rauvala, H., Kaila, K., and Taira, T. (2000). Fast network oscillations in the newborn rat hippocampus in vitro. J. Neurosci. *20*, 1170–1178.

Pape, H.C. (1996). Queer current and pacemaker: the hyperpolarization-activated cation current in neurons. Annu. Rev. Physiol. *58*, 299–327.

Pape, H.C., and McCormick, D.A. (1989). Noradrenaline and serotonin selectively modulate thalamic burst firing by enhancing a hyperpolarization-activated cation current. Nature *340*, 715–718.

Peinado, A. (2000). Traveling slow waves of neural activity: a novel form of network activity in developing neocortex. J. Neurosci. *20*, RC54.

Peinado, A., Yuste, R., and Katz, L.C. (1993). Extensive dye coupling between rat neocortical neurons during the period of circuit formation. Neuron *10*, 103–114.

Raggenbass, M. (2001). Vasopressin- and oxytocin-induced activity in the central nervous system: electrophysiological studies using in-vitro systems. Prog. Neurobiol. *64*, 307–326.

Redmond, L., and Ghosh, A. (2005). Regulation of dendritic development by calcium signaling. Cell Calcium *37*, 411–416.

Roerig, B., and Feller, M.B. (2000). Neurotransmitters and gap junctions in developing neural circuits. Brain Res. Brain Res. Rev. *32*, 86–114.

Rozental, R., Srinivas, M., Gokhan, S., Urban, M., Dermietzel, R., Kessler, J.A., Spray, D.C., and Mehler, M.F. (2000). Temporal expression of neuronal connexins during hippocampal ontogeny. Brain Res. Brain Res. Rev. *32*, 57–71.

Schulz, D.J., Goaillard, J.M., and Marder, E. (2006). Variable channel expression in identified single and electrically coupled neurons in different animals. Nat. Neurosci. *9*, 356–362.

Singer, J.H., Mirotznik, R.R., and Feller, M.B. (2001). Potentiation of L-type calcium channels reveals nonsynaptic mechanisms that correlate spontaneous activity in the developing mammalian retina. J. Neurosci. *21*, 8514–8522.

Sipila, S.T., Huttu, K., Soltesz, I., Voipio, J., and Kaila, K. (2005). Depolarizing GABA acts on intrinsically bursting pyramidal neurons to drive giant depolarizing potentials in the immature hippocampus. J. Neurosci. *25*, 5280–5289.

Sohl, G., Maxeiner, S., and Willecke, K. (2005). Expression and functions of neuronal gap junctions. Nat. Rev. Neurosci. *6*, 191–200.

Spitzer, N.C., Root, C.M., and Borodinsky, L.N. (2004). Orchestrating neuronal differentiation: patterns of Ca2+ spikes specify transmitter choice. Trends Neurosci. *27*, 415–421.

Syed, M.M., Lee, S., Zheng, J., and Zhou, Z.J. (2004). Stage-dependent dynamics and modulation of spontaneous waves in the developing rabbit retina. J. Physiol. *560*, 533–549.

Theodosis, D.T., Koksma, J.J., Trailin, A., Langle, S.L., Piet, R., Lodder, J.C., Timmerman, J., Mansvelder, H., Poulain, D.A., Oliet, S.H., and Brussaard, A.B. (2006). Oxytocin and estrogen promote rapid formation of functional GABA synapses in the adult supraoptic nucleus. Mol. Cell. Neurosci. *31*, 785–794.

Tomizawa, K., Iga, N., Lu, Y.F., Moriwaki, A., Matsushita, M., Li, S.T., Miyamoto, O., Itano, T., and Matsui, H. (2003). Oxytocin improves long-lasting spatial memory during motherhood through MAP kinase cascade. Nat. Neurosci. *6*, 384–390.

Tyzio, R., Ivanov, A., Bernard, C., Holmes, G.L., Ben Ari, Y., and Khazipov, R. (2003). Membrane potential of CA3 hippocampal pyramidal cells during postnatal development. J. Neurophysiol. *90*, 2964–2972.

Tyzio, R., Cossart, R., Khalilov, I., Minlebaev, M., Hübner, C., Represa, A., Ben-Ari, Y., and Khazipov, R. (2006). Maternal oxytocin triggers a transient inhibitory switch in GABA signaling in the fetal brain during delivery. Science *314*, 1788–1792.

Vasilyev, D.V., and Barish, M.E. (2002). Postnatal development of the hyperpolarization-activated excitatory current Ih in mouse hippocampal pyramidal neurons. J. Neurosci. *22*, 8992–9004.

Weissman, T.A., Riquelme, P.A., Ivic, L., Flint, A.C., and Kriegstein, A.R. (2004). Calcium waves propagate through radial glial cells and modulate proliferation in the developing neocortex. Neuron *43*, 647–661.

Wong, R.O., Meister, M., and Shatz, C.J. (1993). Transient period of correlated bursting activity during development of the mammalian retina. Neuron *11*, 923–938.

Yuste, R., Peinado, A., and Katz, L.C. (1992). Neuronal domains in developing neocortex. Science *257*, 665–669.

Yuste, R., Nelson, D.A., Rubin, W.W., and Katz, L.C. (1995). Neuronal domains in developing neocortex: mechanisms of coactivation. Neuron *14*, 7–17.